Bioprinting 15 (2019) e00051

Contents lists available at ScienceDirect

Bioprinting

journal homepage: www.elsevier.com/locate/bprint

Direct 3D bioprinted full-thickness skin constructs recapitulate regulatory signaling pathways and physiology of human skin

Prasad Admane [a], Abhishak C. Gupta [a], Prashanth Jois [b], Subhadeep Roy [a], Chittur Chandrasekharan Lakshmanan [b], Gurpreet Kalsi [b], Balaji Bandyopadhyay [b,**], Sourabh Ghosh [a,*]

[a] Regenerative Engineering Laboratory, Department of Textile Technology, Indian Institute of Technology, Delhi, India
[b] ITC Life Sciences and Technology Centre, ITC Ltd, Bangalore, India

ARTICLE INFO

Keywords:
3D bioprinting
Skin-equivalent
Silk bioink
Signaling pathways

ABSTRACT

Currently available tissue engineered skin-equivalents fail to replicate anatomically relevant features, e.g. undulated morphology of the dermal-epidermal junction, resulting in inadequate recapitulation of biologically meaningful cellular signaling pathways. This study reports fabrication of 3D bioprinted, human cell-based full thickness skin model possessing anatomically relevant structural, mechanical and biochemical features akin to human skin. The unique undulated feature of the epidermis-dermis junction could be recapitulated in the 3D bioprinted skin-equivalents. Extensive migration of the keratinocytes within the construct along with differentiation events reminded reepithelialisation. Cell-cell interaction along with diffusible factors promoted expression of differentiation and cornification markers in region-specific manner. Architectural features and silk bioink microenvironment triggered deposition of basement membrane specific-proteins at the interface. Most interestingly, extensive transcriptomics and proteomics analysis accentuated striking similarity of the 3D bioprinted full thickness skin model to the native human skin, with involvement of a number of pathways related to skin development and physiology, such as skin development, extracellular matrix organization, keratinization/cornification and collagen fibril organization. Such bioprinted *in vitro* human skin models would offer tremendous potential for screening cosmetic products and drugs, as well as to understand the complex physiological processes relevant to human skin thereby bridging the gap between conventional monolayer or 3D cultures and animal models.

1. Introduction

Notable advances have been made in the past to develop tissue engineered human skin-constructs either to repair full thickness skin defects [1–3] or as *in vitro* wound healing models [4] or pathological conditions [5–7]. Tissue engineers have extensively strived to develop three dimensional (3D) engineered skin-equivalents by using advanced biomaterials, cells and various culture techniques to recapitulate the distinctive features that provide skin its unique biological and functional characteristics. However, such skin-equivalents are still lacking in the replication of anatomically relevant undulated morphology of the dermal-epidermal junction (rete ridges), precise alignment of cells and extracellular matrix (ECM) components. Most importantly, the undulated morphology of the dermis-epidermis junction is critical with respect to several key features of the skin namely, 1) providing biochemical cues and mechanical support to the epidermal layer, 2) the adherence of the dermal and epidermal layers; which is crucial for providing structural stability to the skin and most importantly, 3) the migration of cells and diffusion of soluble paracrine factors across the dermal-epidermal junction [8]. Spatial interaction between fibroblasts and keratinocytes control the deposition and turnover of protein composition at the dermal-epidermal interface to form specialized structural features of basement membrane, which is crucial for epidermal differentiation [8] and cell migration in pathological conditions such as epidermolysis bullosa or melanoma [9]. During aging, dermal-epidermal junction gets flattened, whereas in certain pathological conditions, such as psoriasis, rete ridges get lengthened. Unfortunately, most of the previous reports of engineered skin have been based either on 3D porous polymeric scaffolds

* Corresponding author.
** Corresponding author.
E-mail addresses: Balaji.Ban@itc.in (B. Bandyopadhyay), sghosh08@textile.iitd.ac.in (S. Ghosh).

https://doi.org/10.1016/j.bprint.2019.e00051
Received 10 December 2018; Received in revised form 10 March 2019; Accepted 23 April 2019

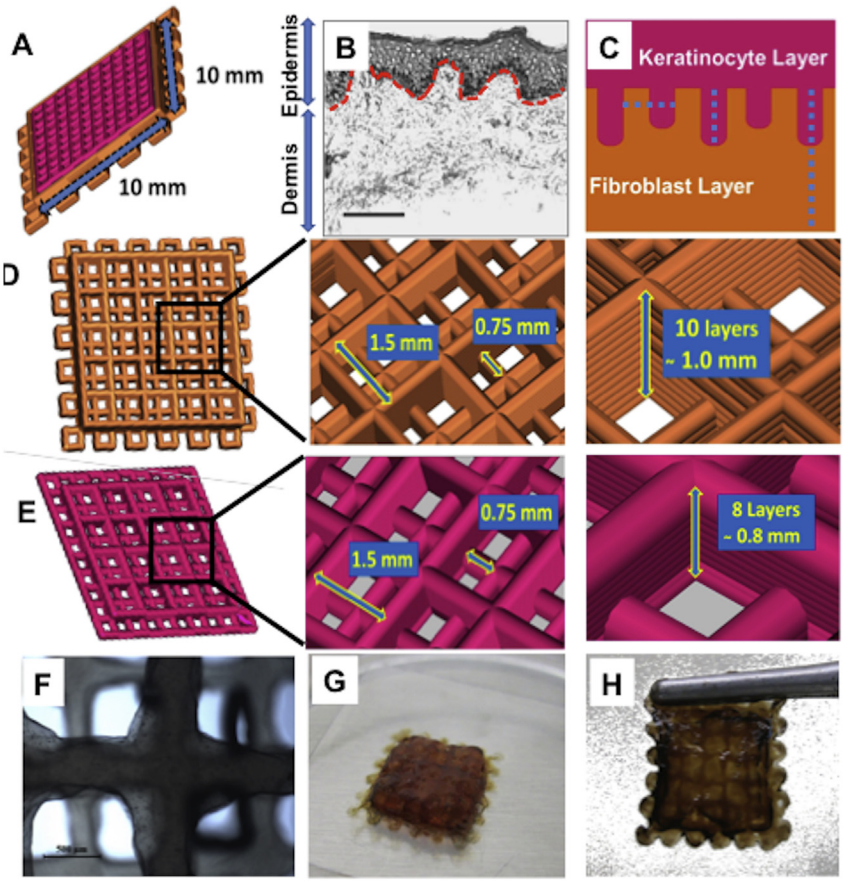

Fig. 1. Schematic representation of the design strategy of the bioinspired, 3D Bioprinted construct. (A) Graphical representation of the Computer Aided Design of the dual layered skin model. The epidermal layer has been designed to invaginate the dermal layer at regular intervals to form rete ridges. (B) Representation of the human skin showing the dermis and epidermis. (C) Structure design strategy for the 10 × 10 mm, dual layered, 3D printed construct. (D and E) Detailed layer design dimensions of the dermal layer and epidermal layers respectively. The dermal layer is constructed of 10 layers and epidermal of 8 layered filaments, arranged perpendicular to each other (in X and Y axes) with interfilament spacing of 0.75 mm and Z axis increment of 0.08 mm between each layer. (F) Microscopic image of the bioprinted construct. (G) Dual layered 10 × 10 mm 3D printed construct in culture. (H) Mechanically stable 3D printed construct offers suitable handling properties for easy characterization.

or transwell-based constructs, which persistently lack in replicating such crucial microstructural details of dermal-epidermal junctions of the human skin. Implantation of such skin-equivalents often results in scar tissue formation. Several reports have highlighted association between abnormal architecture and functioning of basement membrane with hypertrophic scarring [10]. During neo-epithelialization, keratinocytes assume activated phenotype and produce Transforming Growth Factor-β (TGF-β), as well as upregulated expression of keratin 6, 16, and 17 [11]. The soluble factors and/or cytokines secreted by keratinocytes diffuse to the dermis region and induce myofibroblast differentiation due to absence of a proper basement membrane at dermis-epidermis junction in engineered skin constructs. Hence it would be of great interest to fabricate skin-equivalents having undulated morphology of dermis-epidermis junction to decipher valuable insights elucidating the intricate features that are associated with biological functionality of skin-equivalents, namely regeneration, homeostasis and modulation of signaling pathways.

The advent of 3D bioprinting has potential to bring paradigm shift in the field of skin tissue engineering by providing prospects for automated fabrication of structurally complex and physiologically relevant human skin equivalents. 3D bioprinting provides reproducibility with respect to controlled architecture (in terms of size, shape, geometry and orientation), with high precision, while additionally providing options to utilise a variety of bioink material and cell types [12–15]. Wonhye Lee et al. showed development of multi-layered human skin constructs using free form fabrication [16], where the cells retained their morphologies; however low cell viability in the printed constructs was a serious concern. Lee V et al. used inkjet bioprinting for developing 3D skin constructs [17] using collagen bioink. They reported intense N-cadherin expression in the epidermal region, but the expression of markers corresponding to different layers of the skin was not demonstrated. Laser-assisted bioprinting was used to prepare skin construct using NIH3T3 fibroblasts and HaCaT Keratinocytes [18]. The use of immortalized keratinocyte cell line, HaCaT instead of primary human keratinocyte, lead to uncontrolled early differentiation of the cultured cells as opposed to the slow controlled differentiation required for complete stratification of the skin. Du Y et al. used lithographic methods for fabricating multi-layered skin constructs [19]. Cubo N et al. used fibrin-based bioink for printing of primary human cells in form of sheets [20]. However, none of these studies demonstrated the undulated pattern of the dermal-epidermal junction of the human skin.

A range of biomaterials have been utilised as hydrogels in the past to develop 3D bioprinted human skin equivalents namely, collagen [16,17], fibrin [20] or acellular ECM components, e.g., Matriderm [21]. Most of these materials suffer with drawbacks like poor mechanical properties, stability, poor printability etc. Notably, the collagen-based 3D skin equivalents exhibit drastic shrinkage during the 2–3 weeks culture period. Previously, we reported that the silk-gelatin bioink offers excellent printability for fabrication of complex 3D constructs [22] and support long term cell viability. Further, we explored the role of silk fibroin to modulate key signaling pathways responsible for triggering targeted cell differentiation [23,24]. In this study, 3D bioprinting strategies were used for layer-by-layer deposition of the silk-gelatin bioink-laden with the cells (dermal and epidermal) to ultimately generate a multilayered skin-equivalent construct. The use of primary human cells imparts more relevance by appropriately recapitulating the physiological and functional characteristics of human skin. Through extensive analysis of all-encompassing data generated in the current study, we have tried to gain understanding to a number of pertinent questions, 1) the feasibility of fabricating a structural analogue of the epidermal rete ridges and the bilayer model of skin, and the effect of the combined dermal and epidermal cellular interactions towards the functionality of the 3D bioprinted human skin in comparison to the native human skin. 2) How the silk-gelatin bioink and designs of 3D bioprinting govern regulatory

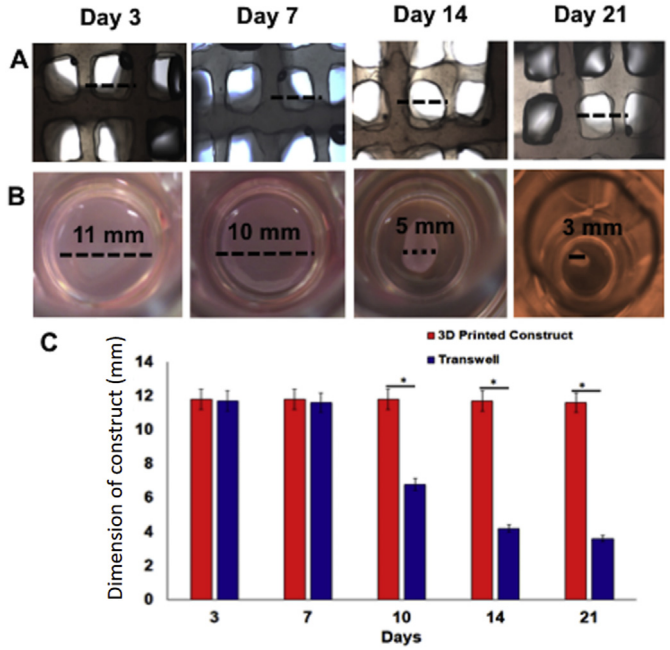

Fig. 2. Stability and swelling studies of the 3D bioprinted constructs. (A) Comparative observation of size, shape and form of the 3D bioprinted construct, where overall dimension of the constuct was preserved over 3 weeks. (B) Conventional collagen transwell experiments showed severe contraction. (C) Comparative graphical representation of the construct dimensions. The 3D bioprinted construct remains stable more than 21 days whereas, the collagen-based construct shows extensive contraction and significant ($P < 0.01$) loss in dimensions at day 10, 14 and 21. The 3D bioprinted construct thus would facilitate long duration experimentation as compared to the conventional transwell culture.

signaling pathways to control cellular polarity and self-assembly. 3) The extent of cellular differentiation in 3D bioprinted human skin model as compared to the native human skin. 4) Most of the earlier studies have been focused on analysis of individual genes or proteins which make it highly challenging for analysis of complex cellular interactions or crosstalks of signaling pathways. To achieve this, we carried out extensive genomics and proteomics analysis to identify the role of complex signaling pathways involved during the dermal-epidermal interface development, keratinocyte differentiation and stratification of the skin in 3D bioprinted skin constructs.

To the best of our knowledge, this forms the first study to report feasibility of automated production using, extrusion-based 3D bioprinting for fabrication of full thickness human skin model showing undulated morphology of epidermal rete ridges, architectural, mechanical and biochemical functionalities similar to human skin. Such bioprinted constructs would prove to be highly applicable for drug or cosmetic testing in comparison to conventional transwell cultures and animal models.

2. Materials and methods

2.1. Cell culture and expansion

Human primary adult dermal fibroblasts were purchased from Himedia (CL005), expanded at a density of 6000 cells/cm^2 in α-MEM (Himedia, ALO80) containing 10% FBS (Hyclone, SH30071.03), 100 U/ml penicillin/streptomycin (Himedia, A001A), 2.5 μg/ml Amphotericin B (Himedia, A011), 50 μg/ml Gentamycin, 5 ng/ml FGF-2 (Prospec, Cyt-218-b) (fibroblast proliferation media) [25]. Human adult keratinocytes were procured from Himedia (CL006), expanded at a cell density of 6000 cells/cm^2 in media containing; DMEM:F12 (1:1), Adenine (180 μM), Insulin (5 μg/ml), Hydrocortisone (0.5 μg/ml), EGF-2 (10 ng/ml), Cholera toxin (10 pg/ml), Penicillin-streptomycin 100 U/ml, Amphotericin 2.5 μg/ml, Gentamicin 50 μg/ml, HEPES (1 ×) and FBS (10%) (keratinocyte proliferation media) [25]. Both the cell types were used within passage 4–5 for all experiments.

2.2. Preparation of silk-gelatin bioink

Silk fibroin-gelatin bioink was prepared following the protocol previously described using 5% w/v silk fibroin and 5% gelatin [24]. Briefly, gelatin was dissolved in the required concentration in the sterilised silk fibroin solution which was held at 37 °C. Media supplements (10 X concentrated Eagle's minimum essential medium, Sigma, M0275) and 10% fetal calf serum were added to support cellular activity. Cells were then suspended in this mixture at desired density. 800 units/ml of mushroom tyrosinase (Sigma-Aldrich T3824-50KU) was added for enzymatic cross-linking. For the dermal component, 2×10^6 cells/ml fibroblasts and for the epidermal component, 5×10^6 cells/ml keratinocytes [17] were mixed with the silk-gelatin bioink.

2.3. 3D CAD model design

3D CAD model was generated using Robocad V 4.0 software (3D Inks LLC, OK, USA) to simulate the dermal and epidermal layers of the human skin. Structures were designed with overall dimensions 10 × 10 mm. The dermal layer consisted of total 14 layers. For initial 5 layers interfilament distance was kept 750 μm. The next 9 layers were designed with filaments in an alternating fashion resulting to interfilament distance 1500 μm to generate a groove like pattern for accommodating the upper epidermal layers. The epidermal structure was formed of total 8 layers with interfilament distance of 1500 μm for the initial 6 layers followed by 750 μm for next 2 layers. The interlayer vertical displacement was kept as of 80 μm for each layer. The alternating grooves formed in the dermal structure helped for formation of a complementary structure representative of the undulated pattern of the dermal-epidermal junction (Fig. 1D and E).

2.4. Preparation of 3D bioprinted constructs

The cell laden silk-gelatin bioink mixture was filled in a sterile 3 ml syringe fitted with a pneumatic piston. Care was taken eliminate air bubbles in the syringe before gelling at 20 °C. The syringe was then fixed on the extrusion head connected with a pressure controlled pneumatic pump. Extrusion was carried out using direct-write assembly (Fiber Align, Aerotech Inc., Pittsburgh, USA) through a 210 μm microcapillary nozzle using the parameters optimised in our previous study [23]. Printing was carried out at 20 ± 2 °C with a speed of 1 mm/s 14 layered dermal constructs were printed with a final height of 2 mm. Bioprinted constructs were incubated at room temperature for 1 h before immersing in fibroblast proliferation media and incubated at 37 °C thereafter. Media was changed every 2 days. After successful analysis of the fibroblast proliferation and ECM deposition at day 3, the epidermal structure was printed on top of the dermal construct. Then the 3D bioprinted constructs were transferred to 1:1 mixture of fibroblast and keratinocyte proliferation media for next 3 days. The dual layered 3D bioprinted constructs were then shifted at air-liquid interface on 12 well transwell inserts (pore size 0.3 μm) for 14 days in a 1:1 mix of fibroblast proliferation: cornification media to allow cornification of the epidermal layer [25].

2.5. Swelling and stability of the bioprinted silk-gelatin constructs in comparison with collagen-based constructs

The filament diameter of the 3D bioprinted constructs (n = 3) was evaluated using Image J (NIH, US) before and after soaking in culture media to calculate the swelling percentage using images captured using Leica Las V3.8. Stability of the 3D bioprinted constructs (n = 3) was

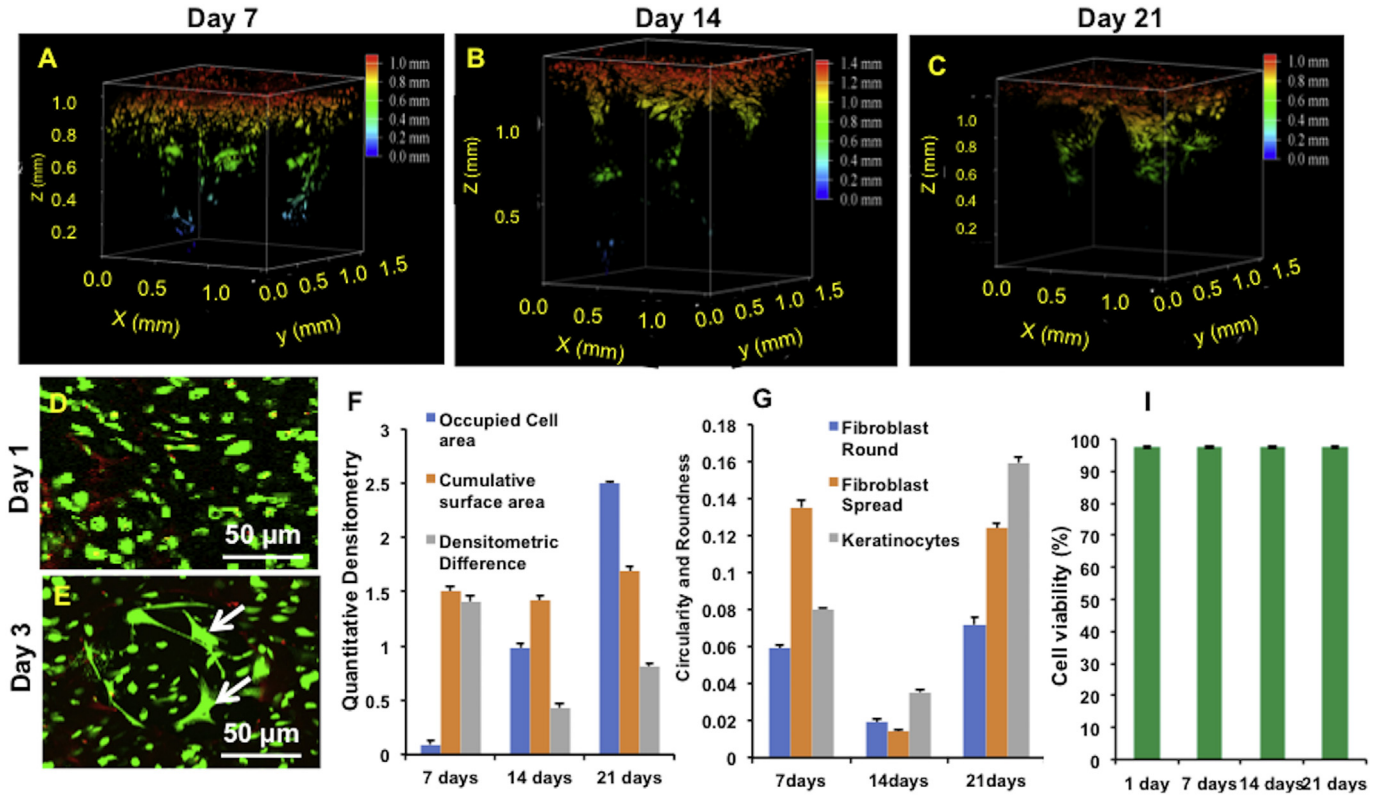

Fig. 3. (A–C) The filaments constituting the epidermal layers fitted on the dermal layers due to structural complementarity to generate an undulated morphology of the dermal-epidermal junction at day 7, 14 and 21. Modulation in fibroblast morphology from round-to-spindle shape in the dermal layer of the 3D bioprinted construct (D) at Day 1 and (E) Day 3. Graphs representing the cellular migration at day 7, 14 and 21 and (F) Cellular morphology such as Roundness, Circularity, Spread (G) and cell viability (I).

assessed based on overall construct dimensions in comparison to the conventional collagen based transwell cultures. Collagen gel-based (2 mg/ml) transwell cultures (n = 3) were established as mentioned earlier [4,26] in 12 well transwell culture plates. The culture conditions with media changes were carried out similar to the bioprinted constructs. The gel dimensions were recorded throughout the culture duration (day 3–21) from images captured using a bright field microscope (Leica).

2.6. Assessment of undulated structures, cellular morphology and migration in the 3D bioprinted silk-gelatin constructs

Morphology and cellular migration of cells in the 3D bioprinted constructs was assessed using the live/dead dye based kit (Invitrogen, USA) by mixing 4 µM ethidium homodimer and 2 µM Calcein AM [24]. Images were captured using confocal microscope (Leica TCS SP5, Leica Microsystems). For quantification of viability, the 3D confocal images were processed using ImageJ for maximum projection by averaging intensity, followed by counting of cells using the multi point utility. Viability was expressed as percentage of viable cells of the total number of cells counted.

Different cell morphologies have been identified by automated score ImageJ standard program feature. Results are reported as mean ± standard deviation, with the shape of at least 100 cells from four independent regions per experimental group being evaluated.

2.7. Gene expression analysis

The bioprinted constructs were digested using 250 µg/ml Protease XIV enzyme (Sigma, P5147) for 20 min at 37 °C to isolate the embedded cells. Cells were separated from the gel debris by centrifugation at 1200 rpm and total RNA was isolated using Trizol (Invitrogen). Quantitative RT-PCR was conducted following the protocol mentioned in our previous study [27] using quantitect primers specific for collagen type 1 alpha (COL1A1, QT00037793), fibronectin (FN1; QT00038024), Laminin-1 (NM_005559). Day 3 3D printed constructs were used as normalizer for all the calculations.

2.8. Total collagen estimation

The total collagen content of the 3D bioprinted constructs (n = 3 for each time point) was measured using hydroxyproline assay [28].

2.9. Immunohistochemistry (IHC)

IHC was carried out to evaluate expression of fibronectin (anti-Fibronectin, 1:200, Abcam), Cytokeratin 1 and Cytokeratin 14 (*anti*-cytokeratin 1, 1:100 Abcam, *anti*-cytokeratin K14, 1:100 Abcam) in the 3D bioprinted constructs using the previously optimised protocol [29]. Alexa Flour 488 conjugated goat anti-mouse IgG antibody (1:200, Invitrogen) and Alexa Fluor 546 conjugated goat anti-mouse IgG (1:200, Invitrogen) were used as secondary antibodies. DAPI (Sigma Aldrich, USA, 32670) was used for nuclear staining. Images were acquired using Leica TCS SP5 (Leica Microsystems) inverted confocal laser scanning microscope.

2.10. Mechanical testing

6 mm × 25 mm 3D bioprinted constructs were fabricated for mechanical tests in comparison to human skin from healthy donor. A special gripping method was devised by using assembly consisted of wooden plates 30 × 10 mm that were bound together with elastic bands to prevent the slipping and rupture of the specimen during tensile testing. The

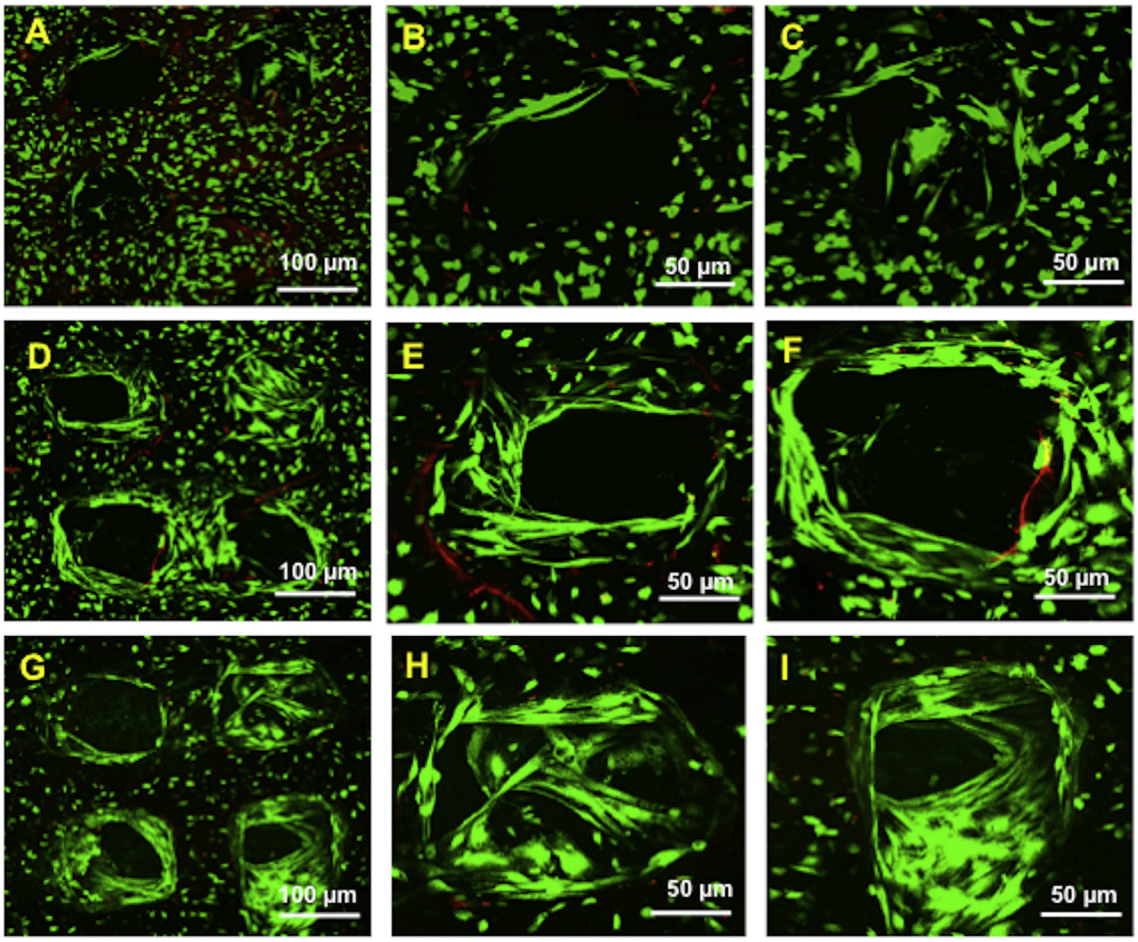

Fig. 4. Extensive migration of the encapsulated keratinocytes, self-assembly and migration towards the pores of the 3D bioprinted construct (A–C) at day 7, (D–F) day 14 and (G–I) day 21 leading to almost completely covered pores, recapitulating re-epithelialization and migration.

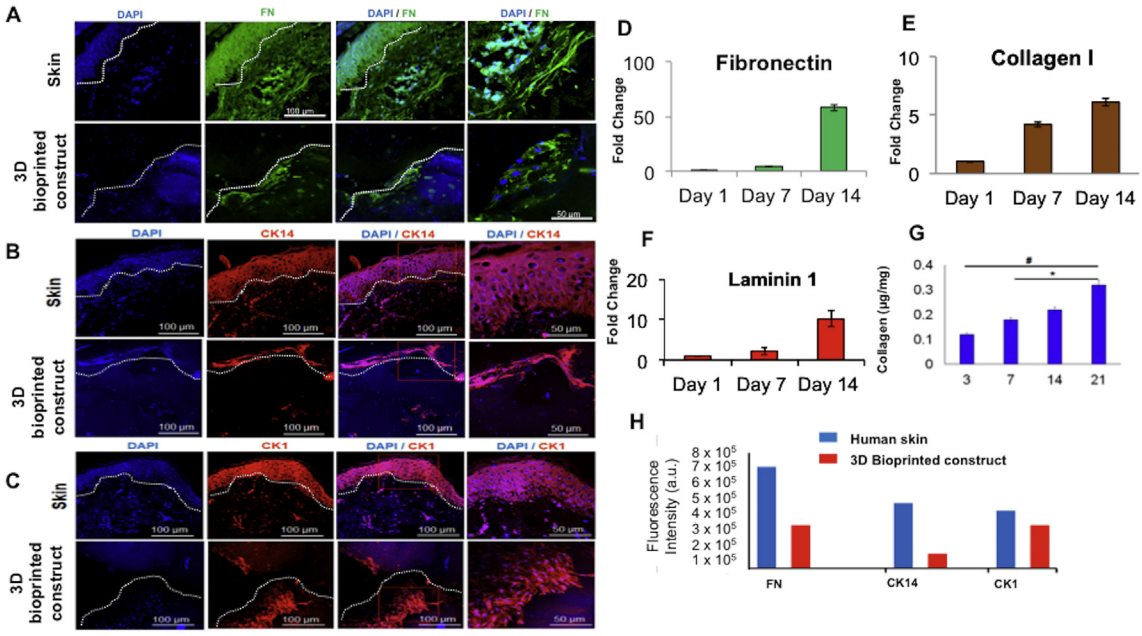

Fig. 5. Immunostaining of (A) Fibronectin (FN), (B) Cytokeratin-14 (CK-14) and (C) Cytokeratin-1 (CK-1) in human skin and 3D bioprinted constructs. Gene expression of FN (D), Collagen type I (E) and Laminin 1 (F) in the 3D bioprinted construct after cornification. (G) Biochemical estimation of the total collagen content, by estimation of hydroxyproline, in the 3D bioprinted constructs. (H) Immunoflourescene intensities of FN, Cytokeratin 14 and 1 in human skin and 3D bioprinted constructs.

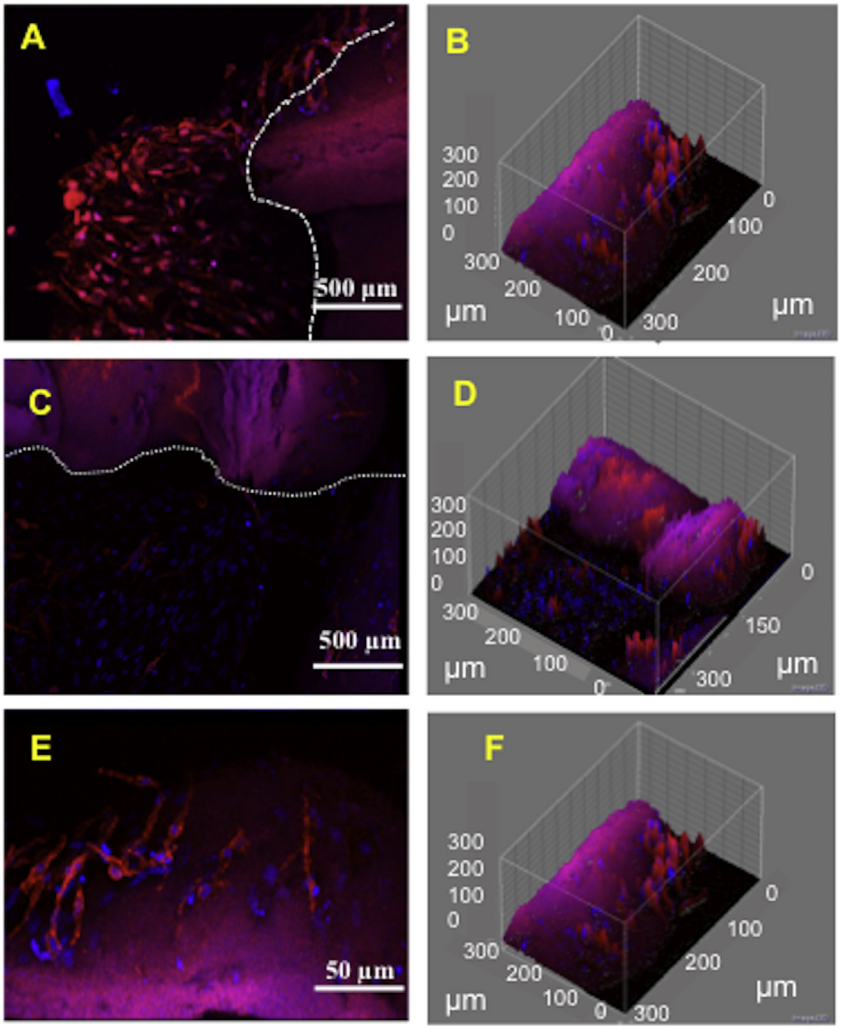

Figure 6. Immunostaining of E-cadherin in the 3D bioprinted constructs. (A) Cytoplasmic as well as localized staining was noticed in the cluster of keratinocytes in epidermal region, indicating cellular adhesion and leading towards barrier formation. Only few cells were found to assume tetrakaidecadedron-like shapes (important marker of barrier effect of skin), which indicates longer time of culture may be required, (B) 3D interactive surface plot showed demarcation of dermal and epidermal junction with the presence of undulated morphology, (C, D) absence of E-cadherin in dermal region, which ensured keratinocytes did not migrate to the dermal layers, (E, F) Cytoplasmic expression was noticed in the keratinocytes which are migratory and displayed extensively elongated morphology. 3D interactive surface plot showed these keratinocytes tend to migrate out of the construct to fill the pores. These cellular features recapitulated proliferation of keratinocytes in the basal layer of human skin to migrate toward stratum spinosum and stratum granulosum.

specimen samples were held in between these plates acting as pads and the grip was adjusted with the help of tension on the elastic bands. The wooden samples were then gripped in the metal jaws of the testing machine (Fig. S2). Evaluation was carried out using Instron 5848 microtester with strain rate 5 mm/min, relative humidity of 50% at 27 °C. The slope of the stress-strain relationship curves was calculated along the linear part of the displacement curve to obtain the Young's modulus. The elongation potential was obtained by maximum strain experienced at the break point.

2.11. Genomic and proteomic analysis

RNA was extracted (as mentioned in the gene expression analysis section) from all the experimental groups namely, 1) 3D bioprinted constructs, 2) Transwell collagen constructs, 3) fibroblasts monolayer, 4) keratinocytes monolayer, 5) monolayer co-culture of fibroblasts and keratinocytes. High-throughput whole transcriptome sequencing (RNA-seq) and Orbitrap based mass spectroscopic analysis were carried out to assess the gene expression and protein expression profiles of human skin vis-à-vis other groups.

Paired-end sequencing was carried out using the NGS platform Illumina HiSeq2000. The Cufflinks program was used to assemble the aligned reads into transcripts, Cuffdiff was used for differential expression analysis. Sequencing of cDNA libraries resulted in generating 25315254 to 34618218 paired-end reads per sample. All high-quality reads were aligned to the human reference genome (mapped to the UCSC hg38 genome build) using TopHat version 2.0.11. Transcript abundance was estimated by calculating FPKM (Fragments per Kilobase of exon per Million fragments mapped) values for gene expression, following which transcript assembly/annotation was performed. Upon applying the 'statistical overrepresentation test' using the 'Panther protein class annotation dataset', several overrepresented protein classes had emerged out ($p < 0.05$, Bonferroni multiple correction). The overlapping set of genes with baseline expression common to both 3D bioprinted human skin model and human skin were analysed for their GO using Panther.

Closeness of 3D bioprinted construct and human skin, was evaluated on the basis of complete protein profiling using Orbitrap. Protein was extracted from the samples following digestion using Protease XIV for 3D bioprinted constructs and Trypsin for monolayer samples. Protein pellet was obtained following centrifugation of isolated cells at 1500 rpm for 5 min and resuspended in lysis buffer (Sigma, C-3228). For human skin samples, approximately 30 mg tissue was homogenized at 5000 rpm for 10 s in lysis buffer. Lysed pellets were maintained on ice for 30 min following centrifugation at 13000 rpm, 15 min. Supernatants were collected and protein estimation was carried out using the micro BCA protein assay kit (Thermo Scientific, Pierce, 23235). Samples were analysed by liquid chromatography–tandem mass spectrometry (LC–MS/MS) using the LTQ Orbitrap and protein dataset for identification (MASCOT). Online software was used for comparative proteomic analysis of proteins identified in all different groups (http://bioinfogp.cnb.csic.es/tools/venny/). Identified proteins were subjected to global

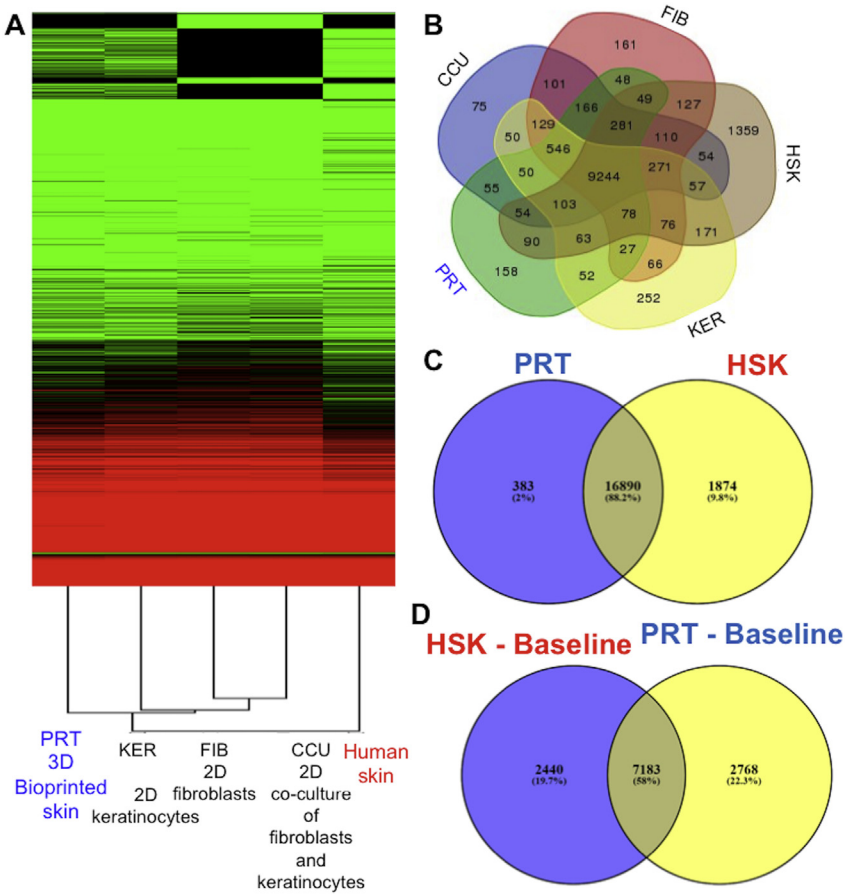

Fig. 7. (A) Unsupervised Hierarchical Condition Tree – at transcript level. Hierarchical clustering-condition for the 5 different samples, FIB (Fibroblasts monolayer), KER (Keratinocyte monolayer), CCU (Monolayer co-culture of fibroblasts and keratinocytes), PRT (3D bioprinted construct) and HSK (human skin). (B) Venn diagram representation of uniquely expressed genes across 5 different samples, FIB, KER, CCU, PRT and HSK. Distribution of uniquely expressed genes (Criteria for expression detection is FPKM ≥ 1) revealed more than 65% of the genes expressed are at baseline (expressed in all the 5 sample profiled) Indicating significant homogeneity in the experiment. Human skin sample shows highest specific gene expression than other groups. (C) Venn diagram representing the distribution of the overall gene expression in the PRT and HSK samples (D) Venn diagram representing the distribution of the baseline expression genes in the PRT and HSK samples.

protein network analysis using STRING tool (Version 10) [30] to obtain information for subsequent functional validation. Functional interpretation was performed to connect the protein identifier with its associated GO terms (http://www.geneontology.org) [31]. Uniprot identifiers proteins were submitted into GO Term Mapper and searched against GOA_human terms for cellular compartment and biological process. The most relevant terms were taken from the GOA and Generic GO slim searches and combined into one file. The numbers of proteins annotated to each term are expressed as a percentage of the total number of Uniprot identifiers submitted into the GO Term Mapper.

2.12. Statistical analysis

All data were presented as mean ± SD and analysed by one way ANOVA followed by Bonferroni's multiple comparison tests with *n* as the number of different experiments. Unpaired *t*-test using Welch's correction was used to estimate the statistical significance for the mechanical tests analysis and one way ANOVA using Tukey's multiple comparison test was applied for gene expression by qRT-PCR. Probability at $p < 0.05$ was considered to be significant. Statistical analysis was carried out using Graph Pad Prism (5.01), San Diego, California, USA.

3. Results and discussion

3.1. Structural stability and design of the 3D bioprinted human skin model

The structural stability of the bioprinted constructs was provided by the enzymatic crosslinking of silk-gelatin using tyrosinase [24], resulting in preservation of structural integrity of the printed constructs until 4 weeks of culture period. Tyrosinase oxidised the tyrosine residues in fibroin and gelatin proteins to form o-quinone moieties that could condense with other amine groups giving rise to inter and intramolecular crosslinks [32]. The construct remained self-sustained while printing, without the need of any external support. The Computer Aided Design (CAD) devised in our study (Fig. 1A,D,E) corresponded to the undulated dermal-epidermal junction morphology of human skin (Fig. 1B). The number of filaments corresponds to different layers as well as governed the depth of the undulated morphology (Fig. 1D). The initial 10 layers of the 3D bioprinted human skin construct represented the dermal component containing the human dermal fibroblast-laden silk-gelatin bioink (Fig. 1D). The subsequent 5 layers of the construct represented the epidermal component with human keratinocytes-laden silk-gelatin bioink (Fig. 1E). The filaments constituting the epidermal layers, fitted on the dermal layers due to structural complementarity to generate a complete bioprinted construct (Fig. 1 G, H), resulting in undulated morphology similar to the dermal-epidermal junction of human skin (Fig. 1A). The individual filaments were seen to undergo 62 ± 2.2% swelling after an incubation of 12 h in media. However, no significant changes in the overall dimensions of the construct were observed even after 21 days (Fig. 2A). The 3D bioprinted construct had spacing between the undulations of rete ridges around 1500 μm (Fig. 2A). The spacing between the undulations of rete ridges in human skin was on an average 100 μm. The average height of the undulation in the native skin tissue and 3D bioprinted construct was 85 ± 5 μm and 500 ± 150 μm respectively.

Stability wise, the transwell collagen constructs (Fig. 2B), in comparison to the 3D bioprinted constructs (Fig. 2A), showed severe contraction (3.6 fold) with time (day 3–21) (Fig. 2C). Collagen-based skin-equivalents have been extensively used, but uncontrolled gelation, poor mechanical properties and severe contraction and collapse during culture duration [33,34] limit utility of such skin constructs and its physiological relevance. In that context, the bioprinted silk-gelatin based

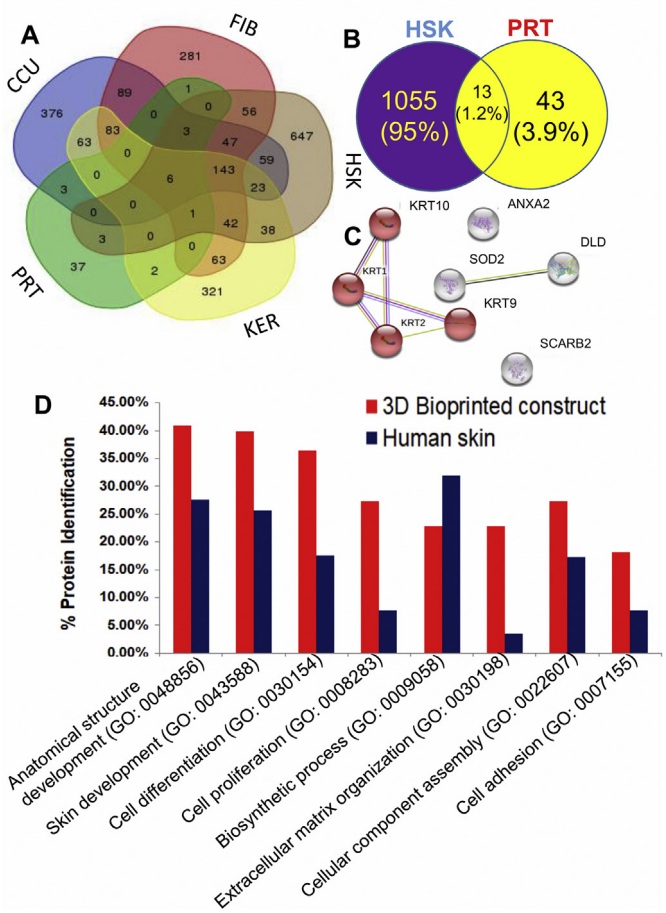

Fig. 8. Venn diagram representation of uniquely expressed proteins across 5 different samples, FIB (Fibroblasts monolayer), KER (Keratinocyte monolayer), CCU (Monolayer co-culture of fibroblasts and keratinocytes), PRT (3D bioprinted construct) and HSK (Human skin) as identified by Orbitrap. (B) Venn Diagram of similar and comparative proteins set in HSK and PRT. (C) STRING analysis of protein–protein interaction of 13 proteins (1.2%) identified in both HSK vs PRT shows keratinocytes differentiation and skin development (KRT: Keratin 1,2,9,10, ANXA2: Annexin A2, SOD2: Superoxide dismutase 2, DLD: Dihydrolipoamide dehydrogenase, SCARB2: Scavenger receptor class B member 2). (D) Comparative gene ontology analysis (GO enrichment analysis) shows major hits of biological process pathways in 3D bioprinted construct and human skin.

constructs could offer major advantage due to preservation of overall dimensions for extended experimental duration, ease of handling. Confocal microscopic images of ethidium homodimer, calcein stained cells within the constructs showed preservation of undulated morphology during the entire culture duration (Fig. 3A–C).

3.2. Evaluation of cellular viability and migration in the 3D bioprinted human skin construct

Viability of the embedded cells was quantified from the images acquired after live/dead staining. The cells embedded in the bioprinted constructs were found to be highly viable (up to 96%) throughout the culture duration (up to 21 days studied) in the bioprinted constructs (Fig. 3I). This observation concluded that the silk-gelatin bioink and the bioprinting parameters supported to maintain high viability of the embedded cells.

Both fibroblasts and keratinocytes were distributed uniformly throughout the 3D bioprinted construct and remodeled their surrounding matrix, changed morphologies during the culture duration. The transition in the morphology of the fibroblast from round to spindle shaped in the dermal layer of the bioprinted constructs during the first 3 days of culture indicated unhindered proliferation of the embedded fibroblasts (Fig. 3D–E) [26]. Quantitative estimation of the degree of spreading and cellular roundness (Fig. 3G) elucidated that the fibroblasts that attained elongated morphology increased by ≈ 1.1 fold ($p < 0.001$) from day 7 to day 21, whereas keratinocytes displayed more elongated morphology (≈3.7 fold) at day 21 as compared to day 7.

Fibroblasts remained embedded within the silk-gelatin bioink, whereas keratinocytes gradually displayed front–rear polarity, probably due to longitudinal adaptation of the actin cytoskeletal structures. Few keratinocytes were also seen to actively migrate out of the constructs after day 7. Most interestingly, extensive migration of the cultured keratinocytes was observed (Fig. 4A–C) towards the pores of the bioprinted construct by day 14 (Fig. 4D–F) that continued till day 21, leading to almost completely covered pores (Fig. 4G–I). After coming out of the spatially constrained situation, these cells at the free edges of the pores of the constructs, drastically reoriented cell polarity. Extensive stretching of actin cytoskeleton and cell polarization for closing of the pores, reminded keratinocytes' migration during re-epithelialization step of wound healing, and maintenance of normal physiological functions of the skin [35]. Primary, differentiated keratinocytes are supposed to be stationary, and may get activated and gain motility during wound healing by inflammatory cytokines or fibrotic cytokines TGF-β or TNF-α and its downstream effector, BMP-2 [36]. Epithelial-to-mesenchymal transition of migrating keratinocytes during wound healing has been extensively studied [37]. After injury, keratinocytes have been known to downregulate epithelial markers E-cadherin and keratins and upregulate mesenchymal markers N-cadherin and vimentin. Hence it was highly interesting to observe extensive keratinocyte migration in porous region of 3D bioprinted constructs, even in the absence of exogenously added growth factors or inflammatory cytokines, which opens up physiological and pathological relevance of the bioprinted skin constructs.

A constellation of factors might be contributing to motility and self-assembly of cells in the 3D bioprinted constructs. Firstly, cellular alignment was initially introduced by the 3D bioprinting process, which triggered patterned signaling to induce single cell polarity. This observation is of utmost significance with respect to the developed *in vitro* human skin model since *in vivo* keratinocyte differentiation and cornification are strongly correlated with the migration and re-epithelisation of keratinocytes [38]. Secondly, the harmony between growth factors and ECM has been well reported to influence keratinocyte motility [35]. We previously reported that silk fibroin component of the bioink helps to retain the soluble factors released by the encapsulated cells within the bioink [39]. Gelatin helps to improve cell adhesion through the exposure of RGD cell adhesion motifs. Rapid proliferation and motility of cells indicated that cells were able to express integrins and form steady focal adhesion contacts with the bioink that helps to develop anchorage with pericellular niche. Thirdly, silk-gelatin bioink is amenable to matrix remodelling by regulation of matrix metalloproteases [39,40], and exposure of cryptic peptides which ultimately lead to migration of the cells. These ECM degradation and matrix remodelling steps are critically dependent on self-assembly of cells [41]. Fourth, keratinocytes growing in the pores showed increased longitudinal tension, which indicates generation of actomyosin-mediated tractional forces due to the higher curvature of cells in the periphery of the pores/empty spaces that promoted keratinocytes to extend and fill the pores. This unique directed migration was unprecedented in the field of 3D bioprinted skin-equivalents and accredited to the delicate balance between engineered guidance by the design of the construct and dynamic remodelling of silk-gelatin bioink by the cells.

3.3. Comparative gene and protein expression analysis of the bioprinted human skin model versus human skin

Fibronectin (FN) and Collagen type I (Col 1) are the major ECM components synthesized by fibroblasts and a hallmark of functional

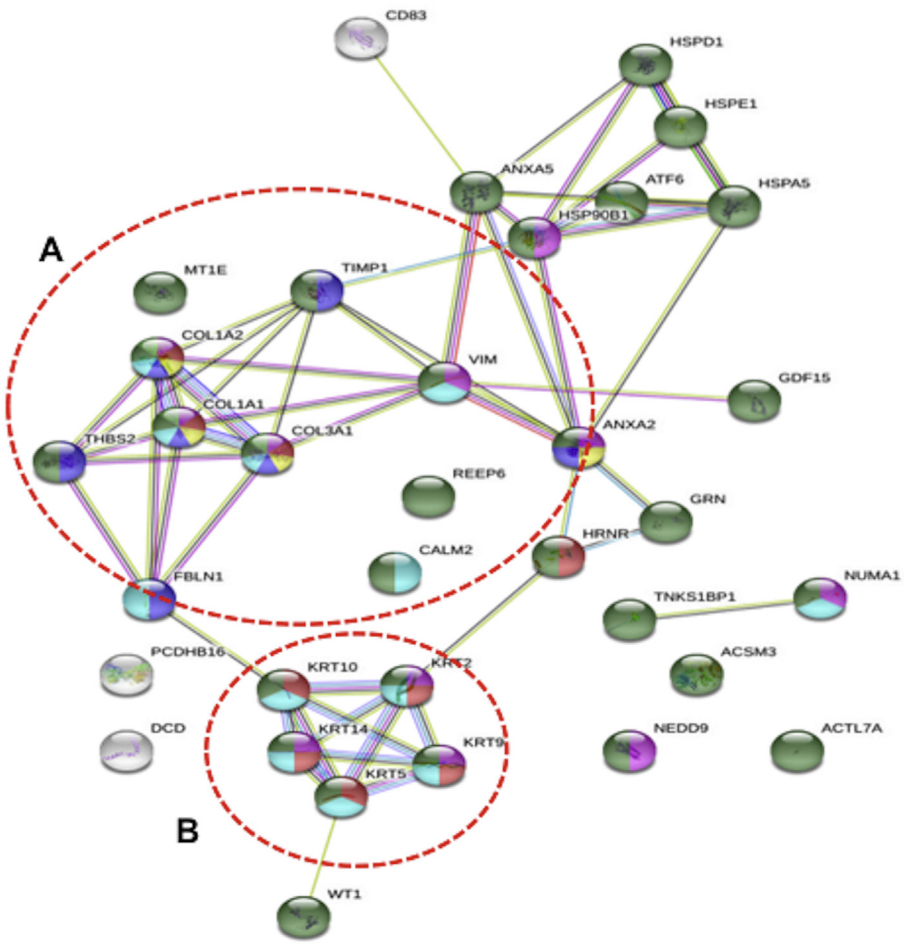

Fig. 9. STRING analysis of protein–protein interaction of 56 proteins show major activated pathways -highlighted circles (A) (Skin Development, Extracellular Matrix organization Keratinization/Cornification and (B) collagen fibril organization in 3D bioprinted construct. Line color indicates the type of interaction evidence, active interactions, colored nodes show query proteins and first shell of interactors. Cellular protein involved in supramolecular fiber organization (pink), skin development (red), collagen fibril organization (yellow), collagen containing extracellular matrix (blue), cytoplasmic part (light green), fibrillar collagen trimer (deep green) function and their intermediate networking. (For interpretation of the references to color in this figure legend, the reader is referred to the Web version of this article.)

Table 1
STRING protein-protein interactions 56 proteins identified in 3D Bioprinted construct showed major hit pathways listed below.

GO-Term	Description
GO:0043588	skin development
GO:0045109	intermediate filament organization
GO:0030198	extracellular matrix organization
GO:0050793	regulation of developmental process
GO:0051239	regulation of multicellular organismal process
GO:0031424	Keratinization
GO:0070268	Cornification
GO:0045684	positive regulation of epidermis development
GO:0030199	collagen fibril organization
GO:0051093	negative regulation of developmental process
GO:0030855	epithelial cell differentiation
GO:0051094	positive regulation of developmental process
GO:0050878	regulation of body fluid levels
GO:0009888	tissue development
GO:0018149	peptide cross-linking
GO:0016043	cellular component organization
GO:0007010	cytoskeleton organization
GO:0048513	animal organ development
GO:0042060	wound healing
GO:0001775	cell activation
GO:2000026	regulation of multicellular organismal development

dermis. FN has proven role in morphogenesis [41] of various organs and cutaneous wound healing [42]. Further, Laminin-1 along with other basement membrane proteins like collagen type IV and VII provide structural stability to the basement membrane [41]. Initially, only the dermal layer was printed with fibroblasts encapsulated in silk-gelatin bioink, which showed extensive upregulation of fibronectin gene expression by 800 fold at day 7, further increase to 900 fold by day 14 and 1600 fold ($p < 0.001$) were observed by day 21 as compared to day 7 and day 14 (Fig. S1A). This was particularly interesting to note because FN expression plays crucial role in scar-less wound healing during gestational period, whereas lower expression during adult wound healing invariably leads to scar formation [43]. However, for the whole 3D bioprinted construct, there was a 60 fold upregulation of FN at day 21 as compared to day 1 (Fig. 5D).

Significant 70 fold upregulation of Col I was observed at day 21 ($p < 0.05$), as compared to day 7 and 14 (Fig. S1B) for the only dermal construct, while the expression of Col I for the 3D bioprinted construct varied from initial 1 fold–5 fold at day 21 (Fig. 5E). Significant 10 fold upregulation of Laminin-1 was observed at day 14 ($p < 0.05$), as compared to day 1 and 7 (Fig. 5F) in the bioprinted construct. Thus such high production of ECM molecules might have significant contribution in the maintenance of the structural stability of our 3D bioprinted skin model. The successive increase in the Col I expression in the 3D bioprinted construct was further validated by the biochemical estimation of hydroxyproline for predicting total collagen content (Fig. 5G). At day 3, total collagen production was minimum with 0.12 μg/mg of construct, gradually rising to 0.16, 0.23 and 0.31 μg/mg at days 7, 14 and 21 respectively (Fig. 5G, significant at $p < 0.05$ as compared to day 3 and day 7). Interestingly, intense staining for distinctly fibrillar FN deposition was evident surrounding the cells at day 14 of the 3D bioprinted constructs (Fig. 5A, Supplementary video) with a distribution akin to the distribution of FN in the native human skin. In human skin, globular FN minimizes the inflammatory response and triggers angiogenesis [44], whereas fibrillar FN plays critical role for tissue repair, provides

structural stability in proteolytic microenvironment (Fig. 5A) [45]. Hence the presence of aligned fibrillar FN in dermal region highlighted parallel contribution of the silk-gelatin bioink and the appropriateness of design of 3D bioprinted construct to recapitulate native skin-like morphology.

Immunofluorescence analysis revealed the expression of basal marker of epidermis (Stratum basale), CK14, which was depictive of proliferative keratinocytes and a distribution similar to expression of CK14 in native human skin (Fig. 5B). Further, differentiation and stratification of keratinocytes is hallmarked by expression of cytokeratins 1 and 10 (CK1 and CK10) (stratum spinosum) [46]. CK1 plays a significant role in regulating inflammatory networks and barrier function in the skin [47]. Expression of CK1 in the 3D bioprinted constructs thus implied maturation and terminal differentiation of the cultured keratinocytes leading to the development of cornified epidermal layer, stratum corneum when cultured at the air-liquid interface (Fig. 5C). Expression of CK14 and CK1 in the present study was in corroboration with the earlier reported skin tissue equivalent developed using human keratinocytes seeded de-epidermized *ex vivo* dermis [5]. The expression of ECM producing genes and differentiation proteins therefore confirms the functionality of the embedded cells in the 3D bioprinted construct and suggests harbouring signatures of skin development.

As extensive motility of keratinocytes is often associated with inverse correlation of E-cadherin expression, we studied E-cadherin localization by immunofluorescence studies. Although, initially homogeneous keratinocyte population was used to fabricate the 3D bioprinted construct but different E-cadherin expression pattern was noticed at different regions of the construct after 21 days. Cluster of keratinocytes were localized in the upper epidermal layer of the constructs (Fig. 6A and B), which showed localized staining around the cell membranes, but dispersed keratinocytes having extended polarized morphology near the pores showed cytoplasmic staining (Fig. 6E and F). Positive E-cadherin expression between cell-cell boundaries correlate to the barrier function to preserve loss of electrolytes and fluids from epidermis of skin and intercellular communication, whereas cytoplasmic localization is correlated to migratory keratinocytes [48].

3.4. Mechanical testing of the 3D bioprinted skin constructs

The skin sample shows the characteristic J-type stress-strain curve as reported earlier [49,50]. This curve distinctively shows the four regions featuring the toe, corresponding to the initial extension at relatively low loads, gradually showing the heel region with increasing slope because of hardening followed by the constant linear slope due to increasing strains which eventually leads to failure. In contrast, the bioprinted skin sample showed a linear pattern from the beginning of the applied strain throughout the elongation process (Fig. S2). Tensile modulus for the native skin (5.25 ± 2.0 MPa) differed significantly as compared to the 3D bioprinted constructs (0.03 ± 0.005 MPa) ($p < 0.05$). Although the modulus of native skin was many fold higher than the 3D bioprinted sample, it was interesting to note that the failure event for both samples was seen after experiencing similar amount of strain. The elongation% at break was similar with no significant difference ($p = 0.4670$) between native skin 58.46 ± 7.31% and 3D bioprinted constructs 65.66 ± 8.54% (Fig. S2). The tensile properties of the skin are majorly dominated by ECM proteins of the dermal component, e.g., collagen and elastin. Presence in high amounts of these fibrous ECM proteins (10% and 4% respectively), orientation and interactions of these fibrous proteins along with hydration level play a major role in imparting the anisotropic mechanical properties to skin [49]. Although, it would be highly challenging to achieve that level, the upcoming bioprinting strategies using modified bioink composition (by blending with other materials and reinforcement of structural fibres, for example elastin in this case, by means of different crosslinking agents) may lead to biomechanically identical skin constructs [51,52].

3.5. Transcriptomics and proteomic data analysis

Detailed transcriptomics and proteomics analysis were conducted in order to identify the complex signaling pathways involved in the regulation of cell-cell and cell-ECM crosstalk in the developed 3D bioprinted human skin model in comparison to the native human skin. The number of expressed transcripts (Expression detection filter, Fragments per Kilobase of exons per million fragments (FPKM) > 1) in the native human skin was higher (17274 transcripts) in comparison with 3D bioprinted human skin model (16211 transcripts), which was as expected considering human skin contains a number of other cell types (such as melanocytes, merkel cells, macrophages and langerhan cells) besides fibroblasts and keratinocytes, thus adding to the total transcript expression. Hierarchical clustering condition tree was prepared for the samples/conditions namely; human skin (HSK), CCU (monolayer co-culture of fibroblast and keratinocytes), FIB (Fibroblast monolayer), KER (Keratinocyte monolayer), PRT (3D bioprinted human skin model) (Fig. 7A).

Pearson Uncentered correlation with average linkage rule revealed that 3D bioprinted construct showed significant similarity with human skin. The distribution of uniquely expressed genes as analysed by GeneVenn (Expression detection filter, FPKM > 1) revealed more than 65% of the genes were expressed at the baseline (expressed in all 5 samples) which further indicated significant homogeneity of the experiment. GeneVenn analysis for the human skin and bioprinted construct revealed 18764 genes expressed in the human skin as compared to the 17273 genes in the bioprinted construct. The distribution of uniquely expressed genes (Expression detection filter, FPKM > 1) revealed that more than 88% of the genes were expressed at the baseline (expressed in both the samples). Upon overlapping these transcripts using GeneVenn, 1874 genes (10%) were differentially expressed in human skin and 383 genes (2%) were differentially expressed in bioprinted construct (Fig. 7C). Further, 9623 genes in human skin and 9951 genes in the bioprinted construct showed baseline expression (Fig. 7D) with 60% similarity in gene expression profile. Gene ontology with PANTHER and GO terms (more than 2 fold differential expression in bioprinted construct as compared to human skin) revealed 228 upregulated genes in bioprinted construct with major role in 1) Collagen binding, 2) ECM structural constituent, 3) Platelet derived growth factor activated receptor activity, 4) Glycosaminoglycan binding, 5) Growth factor binding and 6) Signaling receptor binding. Supplementary Tables 1a and b represents the list of 228 upregulated and 182 downregulated genes (more than 2 fold differential expression) in 3D bioprinted construct as compared to human skin.

1073 proteins were identified in human skin, whereas, 816, 787, 897 and 56 proteins were identified in monolayer culture of fibroblasts, keratinocytes, co-culture and 3D bioprinted construct respectively (Fig. 8). Before going into the detailed analysis it will be noteworthy to mention that there are certainly some differences at transcriptional and translational level, where post translational modifications like proteosomal degradation and/or proteinase activation might contribute to lesser number of identified proteins as compared to genomic analysis as in our study. Furthermore, we cannot exclude the possibility that the final cornification step, during maturation of the bioprinted construct, could possibly be more sensitive to proteolytic machinery corresponding to lesser identified proteins in 3D bioprinted human skin model. Interestingly, few important proteins identified in bioprinted constructs were calmodulin, calcireticulin, Tissue Inhibitor of Metalloproteinase-1 (TIMP-1), keratins (keratins 10, keratin 9, keratin 2) and Annexins (Annexin A2 & Annexin A5) (Supplementary Table 2).

The interactive tool used for comparing the list of proteins provided a comparative protein datasets in each group, which were compared simultaneously for identification of differentially expressed and common proteins in the groups, represented as a circle (set of proteins) (Fig. 8B). 13 (1.2% of total proteins) proteins were observed to be expressed in both human skin and 3D bioprinted construct, which were searched by the STRING tool. The STRING protein-protein interactions clearly

indicated that the 3D bioprinted human skin model showed the major hits corresponding to important regulatory proteins and signaling pathways that play significant role in skin development (Fig. 8C). Comparative generic GO slim searches performed for human skin versus 3D bioprinted construct revealed that the 56 proteins identified in 3D bioprinted construct contributed toward major hits of regulatory pathways that play significant role in skin development (GO:0043588), extracellular matrix organization (GO:0030198), keratinization/cornification (GO:0031424/GO:0070268) and collagen fibril organization (GO:0030199) (Fig. 9 and Table 1). To the best of our knowledge this is the first next generation sequencing study encompassing the detailed genomic and proteomic analysis in a 3D bioprinted human skin model with significant relevant expressions with respect to native human skin [30,31]. Such advanced bioprinted skin construct opens up great possibilities to develop drug/cosmetic screening platform in patient-specific manner, or can further be genetically engineered to establish human dermal pathological models to minimize need of animal clinical trials.

4. Conclusion

The silk-gelatin bioink based 3D bioprinting strategy was used to recapitulate a number of design and biological parameters akin to human skin. Through this study we demonstrated for the first time 1) The bioprinted skin construct was dimensionally stable compared to severe contraction associated with collagen-based skin construct, 2) unique undulated pattern of the dermal-epidermal junction in a 3D bioprinted human skin constructs with physiological relevance to human skin, 3) Extensive migration of the keratinocytes as observed by the complete coverage of the pore of the 3D bioprinted construct by day 21 along with the observed self-assembly of the keratinocytes, 4) Required expression of proliferation and cornification markers depictive of complete stratification of the developed 3D bioprinted human skin model and 4) Extensive transcriptomics and proteomics data analysis showing striking similarity of the developed 3D bioprinted human skin model to human skin involving a number of skin specific and skin development specific pathways. Such successful *in vitro* human skin models have tremendous scope for *in vitro* cosmetics and drug testing and as well for understanding the complex *in vivo* physiological phenomenon. Furthermore, there is scope to develop permeation model to study transdermal behaviour of ingredients/drugs intended to be used for topical application in cosmetic and pharmaceutical industries.

Acknowledgements

Funding support from ITC Ltd. India, is acknowledged.

Appendix A. Supplementary data

Supplementary data to this article can be found online at https://doi.org/10.1016/j.bprint.2019.e00051.

References

[1] S. Ferrari, G. Pellegrini, F. Mavilio, M. De Luca, Gene therapy approaches for epidermolysis bullosa, Clin. Dermatol. 23 (2005) 430–436, https://doi.org/10.1016/j.clindermatol.2004.07.017.
[2] G. Pellegrini, P. Rama, A. Di Rocco, A. Panaras, M. De Luca, Concise review: hurdles in a successful example of limbal stem cell-based regenerative medicine, Stem Cell. 32 (2014) 26–34, https://doi.org/10.1002/stem.1517.
[3] C.M. Reijnders, A. van Lier, S. Roffel, D. Kramer, R.J. Scheper, S. Gibbs, Development of a full-thickness human skin equivalent in vitro model derived from TERT-immortalized keratinocytes and fibroblasts, Tissue Eng. 21 (2015) 2448–2459, https://doi.org/10.1089/ten.tea.2015.0139.
[4] C. Egles, J.A. Garlick, Y. Shamis, Three-dimensional human tissue models of wounded skin, Methods Mol. Biol. 585 (2010) 345–359, https://doi.org/10.1007/978-1-60761-380-0_24.
[5] T.L. Fernandez, D.R. Van Lonkhuyzen, R.A. Dawson, M.G. Kimlin, Z. Upton, Characterization of a human skin equivalent model to study the effects of ultraviolet B radiation on keratinocytes, Tissue Eng. C Methods 20 (2014) 588–598, https://doi.org/10.1089/ten.tec.2013.0293.
[6] P. Eves, C. Layton, S. Hedley, R. a Dawson, M. Wagner, R. Morandini, G. Ghanem, S. Mac Neil, Characterization of an in vitro model of human melanoma invasion based on reconstructed human skin, Br. J. Dermatol. 142 (2000) 210–222.
[7] A.G. Maione, Y. Brudno, O. Stojadinovic, L.K. Park, A. Smith, A. Tellechea, E.C. Leal, C.J. Kearney, A. Veves, M. Tomic-Canic, D.J. Mooney, J.A. Garlick, Three-dimensional human tissue models that incorporate diabetic foot ulcer-derived fibroblasts mimic in vivo features of chronic wounds, Tissue Eng. C Methods 21 (2015) 499–508, https://doi.org/10.1089/ten.tec.2014.0414.
[8] R.E. Burgeson, A.M. Christiano, The dermal-epidermal junction, Curr. Opin. Cell Biol. 9 (1997) 651–658, https://doi.org/10.1016/S0955-0674(97)80118-4.
[9] L. Bruckner-Tuderman, C. Has, Disorders of the cutaneous basement membrane zone-The paradigm of epidermolysis bullosa, Matrix Biol. 33 (2014) 29–34, https://doi.org/10.1016/j.matbio.2013.07.007.
[10] S. Yang, Y. Sun, Z. Geng, K. Ma, X. Sun, X. Fu, Abnormalities in the basement membrane structure promote basal keratinocytes in the epidermis of hypertrophic scars to adopt a proliferative phenotype, Int. J. Mol. Med. 37 (2016) 1263–1273, https://doi.org/10.3892/ijmm.2016.2519.
[11] L. Yang, K. Hashimoto, Y. Shirakata, Epidermogenesis in a skin wound deep through the basement membrane contributes to scar formation, J. Dermatol. Sci. 65 (2012) 224–226, https://doi.org/10.1016/j.jdermsci.2011.10.006.
[12] J. Malda, J. Visser, F.P. Melchels, T. Jüngst, W.E. Hennink, W.J.A. Dhert, J. Groll, D.W. Hutmacher, 25th anniversary article: engineering hydrogels for biofabrication, Adv. Mater. 25 (2013) 5011–5028, https://doi.org/10.1002/adma.201302042.
[13] J. Groll, T. Boland, T. Blunk, J.A. Burdick, D.W. Cho, P.D. Dalton, B. Derby, G. Forgacs, Q. Li, V.A. Mironov, L. Moroni, M. Nakamura, W. Shu, S. Takeuchi, G. Vozzi, T.B.F. Woodfield, T. Xu, J.J. Yoo, J. Malda, Biofabrication, Reappraising the definition of an evolving field, Biofabrication 8 (2016) 013001, https://doi.org/10.1088/1758-5090/8/1/013001.
[14] W.L. Ng, S. Wang, W.Y. Yeong, M.W. Naing, Skin bioprinting: impending reality or fantasy? Trends Biotechnol. 34 (2016) 689–699, https://doi.org/10.1016/j.tibtech.2016.04.006.
[15] P. Benny, C. Badowski, E.B. Lane, M. Raghunath, Making more matrix: enhancing the deposition of dermal–epidermal junction components in vitro and accelerating organotypic skin culture development, using macromolecular crowding, Tissue Eng. 21 (2015) 183–192, https://doi.org/10.1089/ten.tea.2013.0784.
[16] W. Lee, J.C. Debasitis, V.K. Lee, J.H. Lee, K. Fischer, K. Edminster, J.K. Park, S.S. Yoo, Multi-layered culture of human skin fibroblasts and keratinocytes through three-dimensional freeform fabrication, Biomaterials 30 (2009) 1587–1595, https://doi.org/10.1016/j.biomaterials.2008.12.009.
[17] V. Lee, G. Singh, J.P. Trasatti, C. Bjornsson, X. Xu, T.N. Tran, S.-S. Yoo, G. Dai, P. Karande, Design and fabrication of human skin by three-dimensional bioprinting, Tissue Eng. C Methods 20 (2014) 473–484, https://doi.org/10.1089/ten.tec.2013.0335.
[18] L. Koch, A. Deiwick, S. Schlie, S. Michael, M. Gruene, V. Coger, D. Zychlinski, A. Schambach, K. Reimers, P.M. Vogt, B. Chichkov, Skin tissue generation by laser cell printing, Biotechnol. Bioeng. 109 (2012) 1855–1863, https://doi.org/10.1002/bit.24455.
[19] Y. Du, E. Lo, S. Ali, A. Khademhosseini, Directed assembly of cell-laden microgels for fabrication of 3D tissue constructs, Proc. Natl. Acad. Sci. Unit. States Am. 105 (2008) 9522–9527, https://doi.org/10.1073/pnas.0801866105.
[20] N. Cubo, M. Garcia, J.F. del Cañizo, D. Velasco, J.L. Jorcano, 3D bioprinting of functional human skin: production and *in vivo* analysis, Biofabrication 9 (2016) 015006, https://doi.org/10.1088/1758-5090/9/1/015006.
[21] L.E. Fitzpatrick, T.C. McDevitt, Cell-derived matrices for tissue engineering and regenerative medicine applications, Biomater. Sci. 3 (2015) 12–24, https://doi.org/10.1039/C4BM00246F.
[22] S. Chawla, S. Midha, A. Sharma, S. Ghosh, Silk-based bioinks for 3D bioprinting, Adv. Healthc. Mater. 7 (2018) 1701204, https://doi.org/10.1002/adhm.201701204.
[23] S. Das, F. Pati, Y.J. Choi, G. Rijal, J.H. Shim, S.W. Kim, A.R. Ray, D.W. Cho, S. Ghosh, Bioprintable, cell-laden silk fibroin-gelatin hydrogel supporting multilineage differentiation of stem cells for fabrication of three-dimensional tissue constructs, Acta Biomater. 11 (2015) 233–246, https://doi.org/10.1016/j.actbio.2014.09.023.
[24] S. Chawla, A. Kumar, P. Admane, A. Bandyopadhyay, S. Ghosh, Elucidating role of silk-gelatin bioink to recapitulate articular cartilage differentiation in 3D bioprinted constructs, Bioprinting 7 (2017) 1–13, https://doi.org/10.1016/j.bprint.2017.05.001.
[25] M.W. Carlson, A. Alt-Holland, C. Egles, J.A. Garlick, Three-dimensional tissue models of normal and diseased skin (Chapter 19), Curr. Protoc. Cell Biol. (2008), https://doi.org/10.1002/0471143030.cb1909s41. Unit 19.9.
[26] S. Chawla, S. Chameettachal, S. Ghosh, Probing the role of scaffold dimensionality and media composition on matrix production and phenotype of fibroblasts, Mater. Sci. Eng. C 49 (2015) 588–596, https://doi.org/10.1016/j.msec.2015.01.059.
[27] S. Chawla, S. Ghosh, Establishment of in vitro model of corneal scar pathophysiology, J. Cell. Physiol. 233 (2018) 3817–3830, https://doi.org/10.1002/jcp.26071.
[28] M. Bhattacharjee, S. Chawla, S. Chameettachal, S. Murab, N.S. Bhavesh, S. Ghosh, Role of chondroitin sulphate tethered silk scaffold in cartilaginous disc tissue regeneration, Biomed. Mater. 11 (2016) 025014, https://doi.org/10.1088/1748-6041/11/2/025014.
[29] S. Chawla, S. Ghosh, Regulation of fibrotic changes by the synergistic effects of cytokines, dimensionality and matrix: towards the development of an in vitro human dermal hypertrophic scar model, Acta Biomater. 69 (2018) 131–145, https://doi.org/10.1016/j.actbio.2018.01.002.

[30] D. Szklarczyk, A. Franceschini, M. Kuhn, M. Simonovic, A. Roth, P. Minguez, T. Doerks, M. Stark, J. Muller, P. Bork, L.J. Jensen, C. Von Mering, The STRING database in 2011: functional interaction networks of proteins, globally integrated and scored, Nucleic Acids Res. 39 (2011), https://doi.org/10.1093/nar/gkq973.
[31] M. Ashburner, C.A. Ball, J.A. Blake, D. Botstein, H. Butler, J.M. Cherry, A.P. Davis, K. Dolinski, S.S. Dwight, J.T. Eppig, M.A. Harris, D.P. Hill, L. Issel-Tarver, A. Kasarskis, S. Lewis, J.C. Matese, J.E. Richardson, M. Ringwald, G.M. Rubin, G. Sherlock, Gene ontology: tool for the unification of biology, Nat. Genet. 25 (2000) 25–29, https://doi.org/10.1038/75556.
[32] G.D. Kang, K.H. Lee, C.S. Ki, Y.H. Park, Crosslinking reaction of phenolic side chains in silk fibroin by tyrosinase, Fibers Polym. 5 (2004) 234–238, https://doi.org/10.1007/BF02903006.
[33] M.H. Kim, W.H. Park, Chemically cross-linked silk fibroin hydrogel with enhanced elastic properties, Biodegradability, and biocompatibility, Int. J. Nanomed. 11 (2016) 2967–2978, https://doi.org/10.2147/IJN.S106467.
[34] A. Rossi, A. Appelt-Menzel, S. Kurdyn, H. Walles, F. Groeber, Generation of a three-dimensional full thickness skin equivalent and automated wounding, JoVE (2015), https://doi.org/10.3791/52576.
[35] W. Li, G. Henry, J. Fan, B. Bandyopadhyay, K. Pang, W. Garner, M. Chen, D.T. Woodley, Signals that initiate, augment, and provide directionality for human keratinocyte motility, J. Investig. Dermatol. 123 (2004) 622–633, https://doi.org/10.1111/j.0022-202X.2004.23416.x.
[36] C. Yan, W.A. Grimm, W.L. Garner, L. Qin, T. Travis, N. Tan, Y.-P. Han, Epithelial to mesenchymal transition in human skin wound healing is induced by tumor necrosis factor-α through bone morphogenic protein-2, Am. J. Pathol. 176 (2010) 2247–2258, https://doi.org/10.2353/ajpath.2010.090048.
[37] R.C. Stone, I. Pastar, N. Ojeh, V. Chen, S. Liu, K.I. Garzon, M. Tomic-Canic, Epithelial-mesenchymal transition in tissue repair and fibrosis, Cell Tissue Res. 365 (2016) 495–506, https://doi.org/10.1007/s00441-016-2464-0.
[38] I. Pastar, O. Stojadinovic, N.C. Yin, H. Ramirez, A.G. Nusbaum, A. Sawaya, S.B. Patel, L. Khalid, R.R. Isseroff, M. Tomic-Canic, Epithelialization in wound healing: a comprehensive review, Adv. Wound Care 3 (2014) 445–464, https://doi.org/10.1089/wound.2013.0473.
[39] S. Chameettachal, S. Midha, S. Ghosh, Regulation of chondrogenesis and hypertrophy in silk fibroin-gelatin-based 3D bioprinted constructs, ACS Biomater. Sci. Eng. 2 (2016) 1450–1463, https://doi.org/10.1021/acsbiomaterials.6b00152.
[40] C. Egles, Y. Shamis, J.R. Mauney, V. Volloch, D.L. Kaplan, J.A. Garlick, Denatured collagen modulates the phenotype of normal and wounded human skin equivalents, J. Investig. Dermatol. 128 (2008) 1830–1837, https://doi.org/10.1038/sj.jid.5701240.
[41] T. Sakai, M. Larsen, K.M. Yamada, Fibronectin requirement in branching morphogenesis, Nature 423 (2003) 876–881, https://doi.org/10.1038/nature01712.
[42] M.R. Namazi, M.K. Fallahzadeh, R.A. Schwartz, Strategies for prevention of scars: what can we learn from fetal skin? Int. J. Dermatol. 50 (2011) 85–93, https://doi.org/10.1111/j.1365-4632.2010.04678.x.
[43] C.C. Yates, P. Hebda, A. Wells, Skin wound healing and scarring: fetal wounds and regenerative restitution, Birth Defects Res. Part C Embryo Today - Rev. 96 (2012) 325–333, https://doi.org/10.1002/bdrc.21024.
[44] S. Hamed, Y. Ullmann, D. Egozi, E. Daod, E. Hellou, M. Ashkar, A. Gilhar, L. Teot, Fibronectin potentiates topical erythropoietin-induced wound repair in diabetic mice, J. Investig. Dermatol. 131 (2011) 1365–1374, https://doi.org/10.1038/jid.2011.15.
[45] W.S. To, K.S. Midwood, Plasma and cellular fibronectin: distinct and independent functions during tissue repair, Fibrogenesis Tissue Repair 4 (2011) 21, https://doi.org/10.1186/1755-1536-4-21.
[46] M. Moravcová, A. Libra, J. Dvořáková, A. Víšková, T. Muthný, V. Velebný, L. Kubala, Modulation of keratin 1, 10 and involucrin expression as part of the complex response of the human keratinocyte cell line HaCaT to ultraviolet radiation, Interdiscip. Toxicol. 6 (2013) 203–208, https://doi.org/10.2478/intox-2013-0030.
[47] W. Roth, V. Kumar, H.D. Beer, M. Richter, C. Wohlenberg, U. Reuter, S. Thiering, A. Staratschek-Jox, A. Hofmann, F. Kreusch, J.L. Schultze, T. Vogl, J. Roth, J. Reichelt, I. Hausser, T.M. Magin, Keratin 1 maintains skin integrity and participates in an inflammatory network in skin through interleukin-18, J. Cell Sci. 125 (2012) 5269–5279, https://doi.org/10.1242/jcs.116574.
[48] P.V. Peplow, M.P. Chatterjee, A review of the influence of growth factors and cytokines in in vitro human keratinocyte migration, Cytokine 62 (2013) 1–21, https://doi.org/10.1016/j.cyto.2013.02.015.
[49] A. Pissarenko, W. Yang, H. Quan, K.A. Brown, A. Williams, W.G. Proud, M.A. Meyers, Tensile behavior and structural characterization of pig dermis, Acta Biomater. 86 (2019) 77–95, https://doi.org/10.1016/J.ACTBIO.2019.01.023.
[50] R.O. Potts, D.A. Chrisman Jr., E.M. Buras Jr., The dynamic mechanical properties of human skin in vivo, J. Biomech. 16 (1983) 365–372, https://doi.org/10.1016/0021-9290(83)90070-2.
[51] M. McGill, J.M. Coburn, B.P. Partlow, X. Mu, D.L. Kaplan, Molecular and macro-scale analysis of enzyme-crosslinked silk hydrogels for rational biomaterial design, Acta Biomater. 63 (2017) 76–84, https://doi.org/10.1016/j.actbio.2017.09.020.
[52] X. Hu, X. Wang, J. Rnjak, A.S. Weiss, D.L. Kaplan, Biomaterials derived from silk-tropoelastin protein systems, Biomaterials 31 (2010) 8121–8131, https://doi.org/10.1016/j.biomaterials.2010.07.044.